

Azide-Functionalized Nanoclusters via Ligand-Induced Rearrangement

Xi Kang,^{†,‡,§} Mengqi Ren,^{†,§} Manzhou Zhu,^{‡,*} Ke Zhang^{†,*}

[†]Department of Chemistry and Chemical Biology, Northeastern University, Boston, MA 02115, USA.

[‡]Department of Chemistry and Centre for Atomic Engineering of Advanced Materials, Anhui University, Hefei, Anhui 230601, P. R. China.

ABSTRACT: Herein, we report a methodology to prepare atomically precise, azide-functionalized nanoclusters based on ligand-induced rearrangement. Three surface-clickable nanoclusters, including a “waist”-clickable cluster, $\text{Au}_{25}(\text{PPh}_3)_{10}(\text{SPhN}_3)_5\text{Cl}_2$, and two “whole-body” clickable clusters, $\text{Au}_{28}(\text{SPhN}_3)_{20}$ and $\text{Au}_{36}(\text{SPhN}_3)_{24}$, have been prepared and characterized. This work presents a facile and powerful strategy to generate metal nanoclusters with surface ligands of well-defined spatial orientations and numbers, which hopefully can promote various bioconjugation strategies and downstream applications.

Introduction

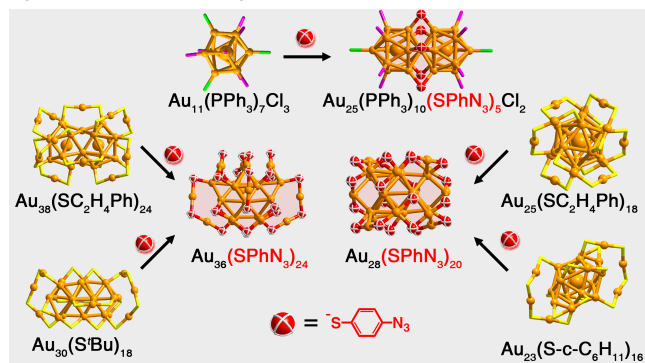
Monolayer-protected metal nanoclusters, also known as ultra-small metal nanoparticles,¹⁻²¹ are an emerging class of modular nanomaterials with atomically precise structures and intriguing physiochemical properties.²²⁻⁴⁷ Many of these properties (fluorescent, catalytic, chiral, and magnetic) have been rationalized as quantum size effects.^{1,9-13,16} The atomically precise nature of nanoclusters allows for the rational fine-tuning of their structures, which gives rise to well-defined material compositions, sizes, and morphologies.^{1,6,15-21}

While several approaches have been reported to manipulate the structure of nanoclusters as well as dictate their properties,^{8,15-21,31,32,38-42,46-65} nanoclusters have in general not been widely adopted for application-driven studies, for example in biomedicine or energy. To build a bridge between the nanocluster synthesis and the applied science communities, it is essential to have an easily adoptable strategy that produces nanoclusters with well-defined peripheral ligands to enable convenient, application-driven modifications. Although nanoclusters with surface carboxylates, amines, and aldehydes have been reported,⁵⁵⁻⁶¹ the coupling efficiency, selectivity, and reaction conditions associated with these functional groups may be unsatisfactory. A more universal strategy starting from well-documented nanoclusters and producing surface ligands containing reliable, highly selective functional groups that can be used for conjugation under mild conditions is still very much desired.

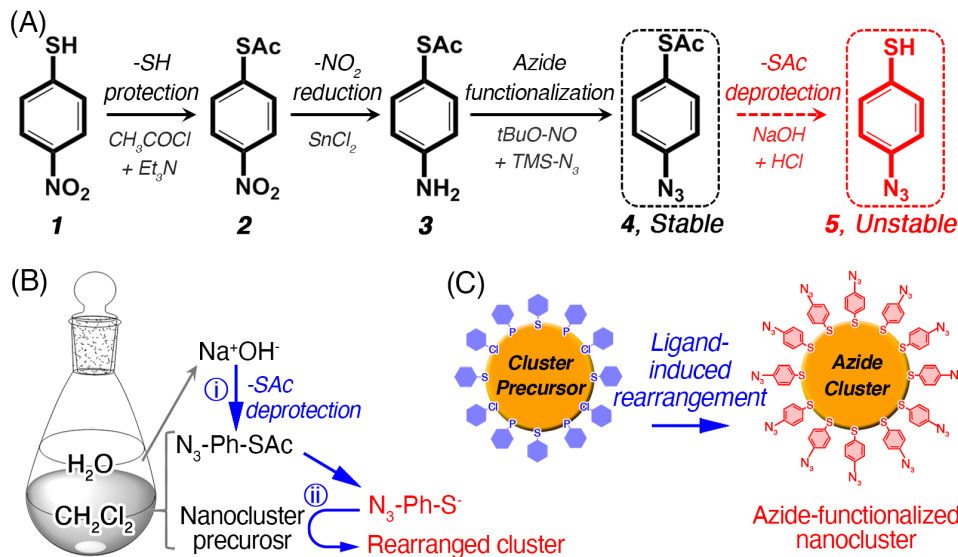
In this work, we take advantage of ligand exchange and subsequent cluster rearrangement to produce azide-functionalized nanoclusters that can be used to conjugate with alkyne-modified ligands via copper-catalyzed or copper-free “click” reactions. The azide-alkyne cycloaddition reaction exhibits exceptional chemoselectivity and works under mild conditions, making it a

highly robust reaction to decorate nanoclusters.⁶²⁻⁶⁵ In our method, *in situ* generated 4-azidobenzenethiol from its acetyl ester is used in a biphasic system to react with pre-synthesized nanocluster precursors. The ligand exchange reaction causes a structural rearrangement of the nanocluster precursors, resulting in new clusters with a different number of gold atoms. In the presence of an excess of 4-azidobenzenethiol, partial exchange of existing phosphine or complete exchange of thiol ligands were observed, both cases leading a pure cluster product represented by a single peak in mass spectrometry. Compositions of these azide-functionalized nanoclusters are determined by electrospray ionization mass spectrometry (ESI-MS) and thermogravimetric analysis (TGA). Three surface-clickable nanoclusters, including $\text{Au}_{25}(\text{PPh}_3)_{10}(\text{SPhN}_3)_5\text{Cl}_2$, $\text{Au}_{28}(\text{SPhN}_3)_{20}$, and $\text{Au}_{36}(\text{SPhN}_3)_{24}$ were prepared and characterized (Scheme 1).

Scheme 1. Transformation of gold nanoclusters to new ones via ligand-induced rearrangement.



Scheme 2. Preparation of azide-functionalized nanoclusters. (A) Synthesis of ligand. (B) A biphasic system for *in situ* ligand generation and ligand-induced rearrangement. (C) Schematic representation of the overall transformation.



Experimental Section

Materials and Methods. All reagents were purchased from Sigma-Aldrich or Fisher Scientific and used without further purification. Nanocluster precursors, including $\text{Au}_{11}(\text{PPh}_3)_7\text{Cl}_3$, $\text{Au}_{23}(\text{S}-c\text{-C}_6\text{H}_{11})_{16}$, $\text{Au}_{25}(\text{SC}_2\text{H}_4\text{Ph})_{18}$, $\text{Au}_{30}(\text{S}-t\text{-C}_4\text{H}_9)_{18}$, and $\text{Au}_{38}(\text{SC}_2\text{H}_4\text{Ph})_{24}$, were synthesized based on reported methods.^{66, 70}

Preparation of ligand precursor (4, Scheme 2). To a stirred solution of 4-nitrobenzenethiol (1, 516 mg, 3.33 mmol) and 689 μL triethylamine in dichloromethane (10 mL) was dropwise added a solution of acetyl chloride (314 mg, 4 mmol) in dichloromethane (5 mL) at 0 °C. The reaction was slowly raised to room temperature and stirred overnight. The mixture was quenched with methanol (2 mL) for 30 min and diluted by ethyl acetate (200 mL) and rinsed by saturated NaHCO_3 (200 mL 3×) and brine (200 mL 3×). The organic phase was dried by Na_2SO_4 , filtered, and concentrated by a rotary evaporator. The residue was purified by flash column chromatography with hexane/ethyl acetate (50:50 v:v) as eluent to give a pale yellow solid of *S*-(4-nitrophenyl) ethanethioate (2, 435 mg, 84%). ¹H NMR (CDCl_3) δ 8.25 (d, J = 8.7 Hz, 2H), 7.60 (d, J = 8.7 Hz, 5H), 2.49 (s, 3H). ¹³C NMR (100 MHz, CDCl_3) δ 191.46, 146.87, 136.84, 134.71, 123.83, 30.44. LC-ESI (m/z): [M+H]⁺ calcd for $\text{C}_8\text{H}_8\text{N}_3\text{OS}^+$ 194.0, found 198.0.

Next, 2 (591 mg, 3 mmol), anhydrous SnCl_2 (5.69 g, 30 mmol), and ethanol (30 mL) were mixed in a 50mL Schlenk flask. The reaction was stirred at 60 °C under nitrogen for 2 hours. After completion of the reaction (monitored by TLC; R_f of 3 is ~0.6 with of 50:50 v:v hexane:ethyl acetate), NaOH aqueous solution (1 M) was dropwise added to the reaction mixture until the pH reaches around 9, and 200 mL water was added. The crude product precipitated and was extracted by ethyl acetate (200 mL 3×). The combined organic layers were dried by Na_2SO_4 and concentrated to give a yellow solid of *S*-(4-aminophenyl) ethanethioate (3, 443 mg, 88%). The crude product was directly used for next step without purification.

Next, to a stirred solution of 3 (225 mg, 1 mmol) in dichloromethane (5 mL) was dropwise added a solution of *tert*-butyl

nitrite (180 μL , 1.5 mmol) in acetonitrile (1 mL) at 0 °C under nitrogen. After stirring for 5 minutes, a solution of trimethylsilyl azide (160 μL , 1.2 mmol) in acetonitrile (1 mL) was dropwise added to the mixture. The reaction was stirred for a further 30 minutes at 0 °C. The mixture was then concentrated and purified by a flash column chromatography with hexane:ethyl acetate (75:25 v:v) to yield a yellow oil of *S*-(4-azidophenyl) ethanethioate (4, 131 mg, 68%). ¹H NMR (CDCl_3) δ 7.38 (d, 2H), 7.07 (d, 2H), 2.42 (s, 3H). ¹³C NMR (CDCl_3) δ 194.07, 141.70, 136.03, 124.11, 119.86, 30.17. LC-ESI (m/z): [M+H]⁺ calcd for $\text{C}_8\text{H}_8\text{N}_3\text{OS}^+$ 194.0, found 194.1.

Preparation of azide-functionalized nanoclusters. To a CH_2Cl_2 solution of nanocluster precursor (2 mg of cluster in 1 mL of CH_2Cl_2), 20 mg of 4 was added under stirring. Then, 1 mL of aqueous solution containing 5 mg of NaOH was added. The azide-thiol is in large excess (200×) to ensure complete reaction. After 2 hours, the organic phase was precipitated into 20 mL of *n*-hexane. The precipitation was re-dissolved in CH_2Cl_2 , which contained the azide-functionalized nanoclusters. The yields for the preparation of azide-functionalized nanoclusters (based on the Au element) were as follows: $\text{Au}_{11}(\text{PPh}_3)_7\text{Cl}_3$ precursor, 60%; $\text{Au}_{23}(\text{S}-c\text{-C}_6\text{H}_{11})_{16}$ precursor, 50%; $\text{Au}_{25}(\text{SC}_2\text{H}_4\text{Ph})_{18}$ precursor, 60%; $\text{Au}_{30}(\text{S}-t\text{-C}_4\text{H}_9)_{18}$, 30%; $\text{Au}_{38}(\text{SC}_2\text{H}_4\text{Ph})_{24}$ precursor, 80%.

Click reaction between nanoclusters and a model cyclooctyne ligand. To a CH_2Cl_2 solution of $\text{Au}_{28}(\text{SPh}_3)_{20}$ (8 mg of cluster in 3 mL of CH_2Cl_2), 5 mg of 5-hydroxy-1,2:5,6-dibenzocyclooct-7-yne (abbreviated as DBCO-OH) was added under stirring. The mixture was stirred at 40 °C for 2 hours. Thereafter, the reaction mixture was precipitated into 20 mL of *n*-hexane. The precipitate was determined to be $\text{Au}_{28}(\text{SPh}_3\text{-DBCO-OH})_{20}$ (11.5 mg). The yield of the reaction is 95%.

Results and Discussion

In the past few years, the ligand exchange method has been extensively applied for the preparation of new nanoclusters.^{50,51} It is accepted that (i) the ligand exchange process can transform the configuration of nanoclusters by substituting their surface ligands, and (ii) the structure of the new nanocluster is largely dependent on the starting cluster.^{50,51} To prepare azide-functionalized

nanoclusters, a small, rigid thiol-containing ligand, 4-azidobenzenethiol (**5** in Scheme 2), is designed. However, the azide thiol itself is unstable at room temperature. Therefore, the *S*-acetylated ligand is used to generate the free thiol *in situ* in the presence of sodium hydroxide (Scheme 2). The acetylated ligand is synthesized in three steps from 4-nitrobenzenethiol (**1**). Briefly, **1** is reacted with acetyl chloride to yield *S*-(4-nitrophenyl) ethanethioate (**2**), which is then reduced by SnCl_2 to generate *S*-(4-aminophenyl) ethanethioate (**3**). Finally, the aromatic amine is converted to an azide, *S*-(4-azidophenyl) ethanethioate (**4**), in one pot with *tert*-butyl nitrite and trimethylsilyl azide.⁷¹ Several efforts were made to

deprotect the thioester to generate the target thiol **5**; however, **5** was unstable likely because of spontaneous rearrangement (Figure S3A). Instead, a biphasic system was set up to generate **5** *in situ*, which can then react with the nanocluster (Scheme 2B). Specifically, **4** and a nanocluster precursor are first dispersed in the CH_2Cl_2 ; under vigorously stirring, an aqueous solution of NaOH is added. The deprotection of the thioester occurs at the $\text{H}_2\text{O}/\text{CH}_2\text{Cl}_2$ interface, sparing the nanocluster from the strong basic deprotection conditions, and the resulting **5** immediately participates in the reaction.

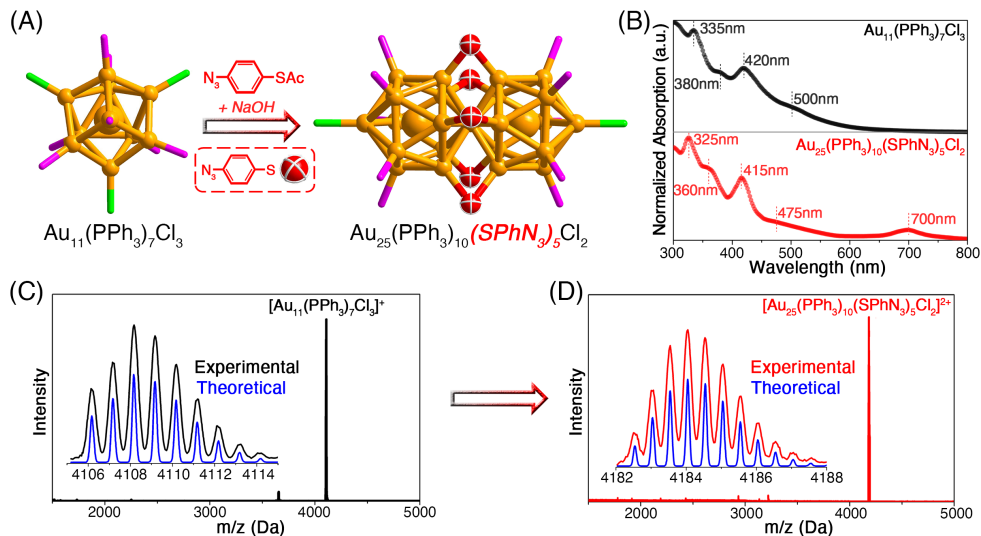


Figure 1. Preparation of $\text{Au}_{25}(\text{PPh}_3)_{10}(\text{SPhN}_3)_5\text{Cl}_2$. (A) Schematic illustration of the overall reaction. Color codes: orange, Au; purple, P; green, Cl; red, S. For clarity, all C and H atoms are omitted. (B) UV-vis spectra of $\text{Au}_{11}(\text{PPh}_3)_7\text{Cl}_3$ and $\text{Au}_{25}(\text{PPh}_3)_{10}(\text{SPhN}_3)_5\text{Cl}_2$. (C, D) ESI-MS results of $\text{Au}_{11}(\text{PPh}_3)_7\text{Cl}_3$ and $\text{Au}_{25}(\text{PPh}_3)_{10}(\text{SPhN}_3)_5\text{Cl}_2$. Insets: experimental and calculated isotope patterns for each nanocluster.

We first tested our ligand exchange method with $\text{Au}_{11}(\text{PPh}_3)_7\text{Cl}_3$ as the nanocluster precursor, which has a defective icosahedral configuration (Figure 1A).⁶⁶ ESI-MS and UV-vis spectroscopy were performed to track the ligand exchange process. As shown in Figure 1B, the CH_2Cl_2 solution of $\text{Au}_{11}(\text{PPh}_3)_7\text{Cl}_3$ exhibited two absorptions at 335 and 420 nm, and two shoulder bands at 380 and 500 nm. After ligand exchange, the resulting nanocluster displayed a distinctive sequence of optical absorptions at 325, 360, 415, 475, and 700 nm, which are reminiscent of the optical characteristics of the rod-like Au_{25} nanocluster (i.e., $\text{Au}_{25}(\text{PPh}_3)_{10}(\text{SR})_5\text{Cl}_2$).⁷² However, the last peak at 700 nm showed a ~ 30 nm red-shift relative to typical rod-like Au_{25} clusters.⁷² ESI-MS of the precursor cluster showed a mass peak at m/z of 4108.2 Da (Figure 1C). After ligand exchange, a peak at m/z of 8368.2 Da arose, which can be perfectly assigned to $[\text{Au}_{25}(\text{PPh}_3)_{10}(\text{SPhN}_3)_5\text{Cl}_2]^{2+}$ (Figure 1D). TGA showed a weight loss of 41.85%, which was consistent with the calculated loss (41.66%) of PPh_3 , SPhN_3 , and Cl ligands/counterions in the assigned formula (Figure S4). Fourier-transform infrared (FTIR) spectrum of the nanocluster exhibited a distinctive azide vibration at 2135 cm^{-1} , confirming the presence of the new azide ligand (Figure S5). Elemental analysis (EA) also confirmed the proposed composition (Table S1). Such conversion from mono-icosahedral Au_{11} clusters to bi-icosahedral Au_{25} clusters has been reported previously.⁷² Although the crystal structure of $\text{Au}_{25}(\text{PPh}_3)_{10}(\text{SPhN}_3)_5\text{Cl}_2$ is not obtained in this study, we propose a

structure based upon optical properties and the empirical formula of $\text{Au}_{25}(\text{PPh}_3)_{10}(\text{SR})_5\text{Cl}_2$,⁷² where five thiol atoms and a shared gold atom bridge two Au_{13} icosahedra to form a rod-like structure (Figure 1A).

Next, the ligand exchange reaction was performed on two nanoclusters, $\text{Au}_{23}(\text{S}-c\text{-C}_6\text{H}_{11})_{16}$ and $\text{Au}_{25}(\text{SC}_2\text{H}_4\text{Ph})_{18}$ (Figure 2), which are stabilized by thiol ligands instead of phosphine ligands. Interestingly, both clusters produced identical optical and ESI-MS results after ligand exchange (Figure 2B-C). UV-vis spectroscopy revealed a prominent peak at 375 nm, and two shoulder bands at 480 and 605 nm (Figure 2B, red). The product has an m/z of 8650.2 Da, corresponding to a formula of $[\text{Au}_{28}(\text{SPhN}_3)_{20}\text{Cs}]^+$. TGA showed a weight loss of 35.06%, consistent with the composition of $\text{Au}_{28}(\text{SPhN}_3)_{20}$ (Figure S6). Again, FTIR showed the characteristic azide vibration at 2135 cm^{-1} (Figure S7), confirming the presence of the azide thiol. Based on these findings, we postulate that the newly formed nanocluster is structurally analogous to $\text{Au}_{28}(\text{SPhBu})_{20}$, which has similar optical properties.^{73,74} The newly obtained $\text{Au}_{28}(\text{SPhN}_3)_{20}$ nanocluster exhibits 20 surface clickable sites across the entire particle surface (Figure 2A, middle). These studies suggest the ligand exchange process is able to disrupt the thermodynamic equilibrium of the precursor clusters, leading to complete structural rearrangement and a new, lower-energy product despite two different starting points.

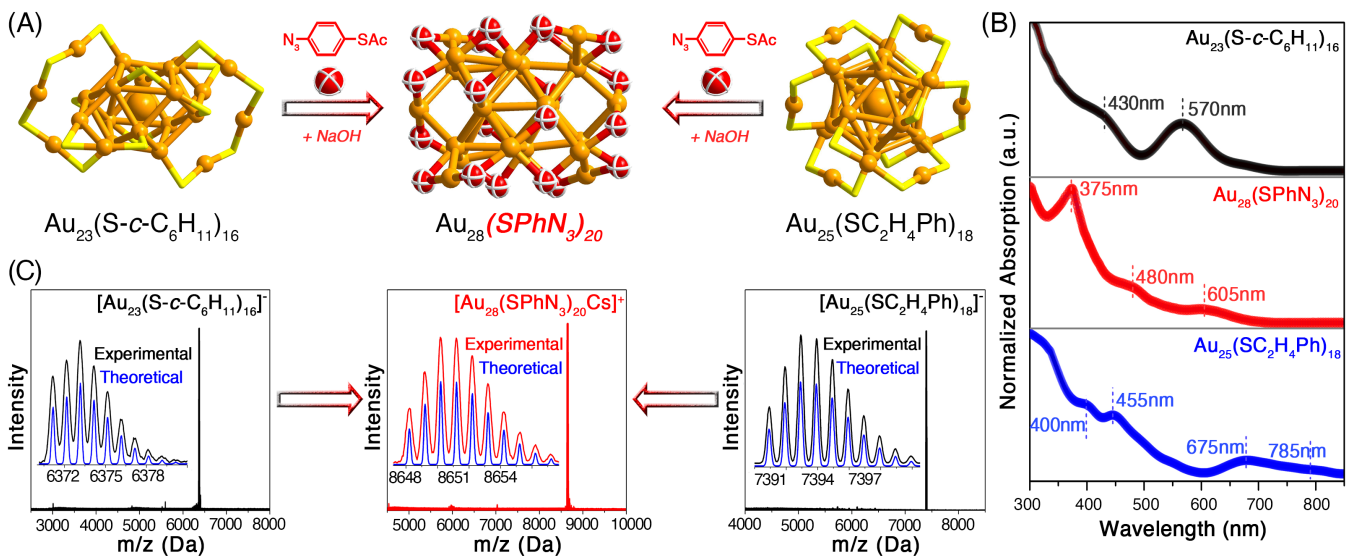


Figure 2. Preparation of $\text{Au}_{28}(\text{SPhN}_3)_{20}$. (A) Schematic illustration of the overall reaction. Color codes: orange, Au; yellow, S. (B) UV-vis spectra of $\text{Au}_{23}(\text{S}-\text{c-C}_6\text{H}_{11})_{16}$, $\text{Au}_{25}(\text{SC}_2\text{H}_4\text{Ph})_{18}$, and $\text{Au}_{28}(\text{SPhN}_3)_{20}$. (C) ESI-MS results of $\text{Au}_{23}(\text{S}-\text{c-C}_6\text{H}_{11})_{16}$, $\text{Au}_{25}(\text{SC}_2\text{H}_4\text{Ph})_{18}$, and $\text{Au}_{28}(\text{SPhN}_3)_{20}$. Insets: experimental and calculated isotope patterns for each nanocluster.

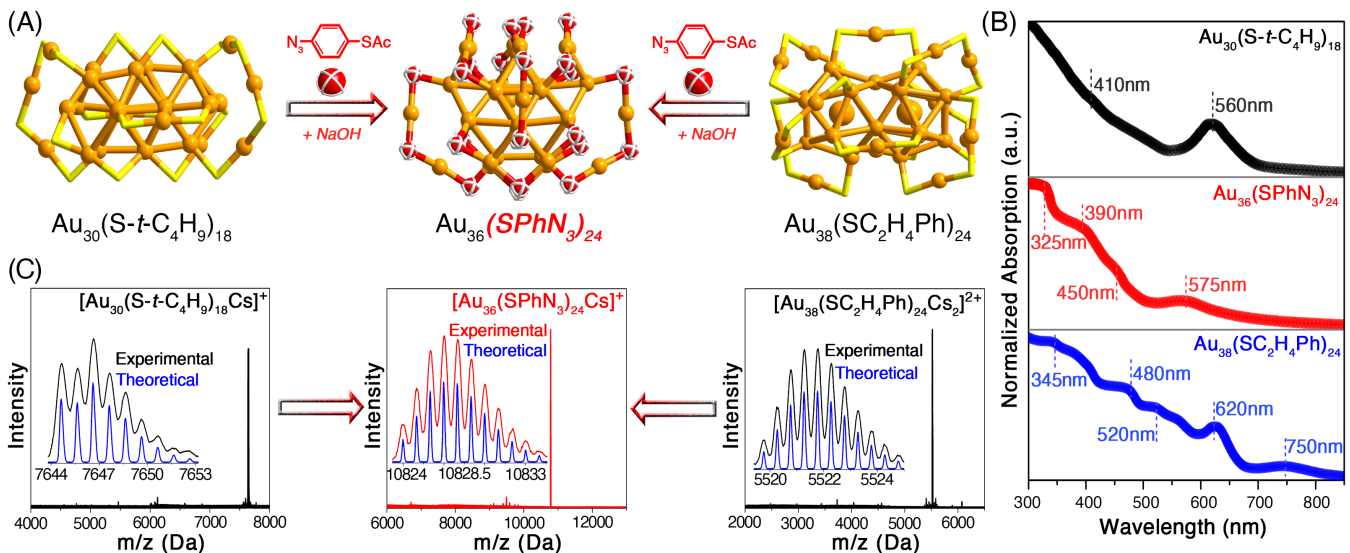


Figure 3. Preparation of $\text{Au}_{36}(\text{SPhN}_3)_{24}$. (A) Schematic illustration of the overall reaction. Color codes: orange, Au; yellow, S. (B) UV-vis spectra of $\text{Au}_{30}(\text{S}-\text{t-C}_4\text{H}_9)_{18}$, $\text{Au}_{36}(\text{SPhN}_3)_{24}$, and $\text{Au}_{38}(\text{SC}_2\text{H}_4\text{Ph})_{24}$. (C) ESI-MS results of $\text{Au}_{30}(\text{S}-\text{t-C}_4\text{H}_9)_{18}$, $\text{Au}_{36}(\text{SPhN}_3)_{24}$, and $\text{Au}_{38}(\text{SC}_2\text{H}_4\text{Ph})_{24}$. Insets: experimental and calculated isotope patterns for each nanocluster.

We further applied the ligand exchange reaction to two larger nanoclusters, $\text{Au}_{30}(\text{S}-\text{t-C}_4\text{H}_9)_{18}$ and $\text{Au}_{38}(\text{SC}_2\text{H}_4\text{Ph})_{24}$ (Figure 3). Again, UV-vis spectroscopy of the resulting nanoclusters exhibited identical main absorptions at 325 and 575 nm as well as shoulder bands at 390 and 450 nm (Figure 3B, red). In addition, both products exhibited an m/z of 10827.0 Da as determined by ESI-MS, indicating the formula of $[\text{Au}_{36}(\text{SPhN}_3)_{24}\text{Cs}]^+$ (see the matching experimental and calculated isotope patterns in Figure 3C, middle), which was further supported by EA, TGA and FTIR characterization (Figures S8-9). In light of (i) the comparable metal-ligand compositions and analogous optical absorptions between $\text{Au}_{36}(\text{SPhN}_3)_{24}$ and the previous reported $\text{Au}_{36}(\text{SPh}^{\prime}\text{Bu})_{24}$,⁷⁵ (ii) the similar structure between -SPhN₃ and -SPh'Bu ligands, the structure of $\text{Au}_{36}(\text{SPhN}_3)_{24}$ is speculated based on the known structure of $\text{Au}_{36}(\text{SPh}^{\prime}\text{Bu})_{24}$ (Figure 3A), where 24 surface-clickable azides

emanate from the entire surface of the nanocluster. Indeed, the nanocluster transformations from $\text{Au}_{30}(\text{S}-\text{t-C}_4\text{H}_9)_{18}$ to $\text{Au}_{36}(\text{SPh}^{\prime}\text{Bu})_{24}$ and from $\text{Au}_{38}(\text{SC}_2\text{H}_4\text{Ph})_{24}$ to $\text{Au}_{36}(\text{SPh}^{\prime}\text{Bu})_{24}$ have been documented previously.⁷⁵⁻⁷⁷ All azide-functionalized nanoclusters reported here display a different size relative to their precursors, which suggests that the activation energy for nanoclusters to rearrange is quite low, and that the structure/composition of the rearranged nanocluster are strongly dependent on the new surface ligands.⁵¹ These results also imply that ligand exchange without affecting the overall nanocluster structure may be challenging, unless the starting precursor is a highly stable one.

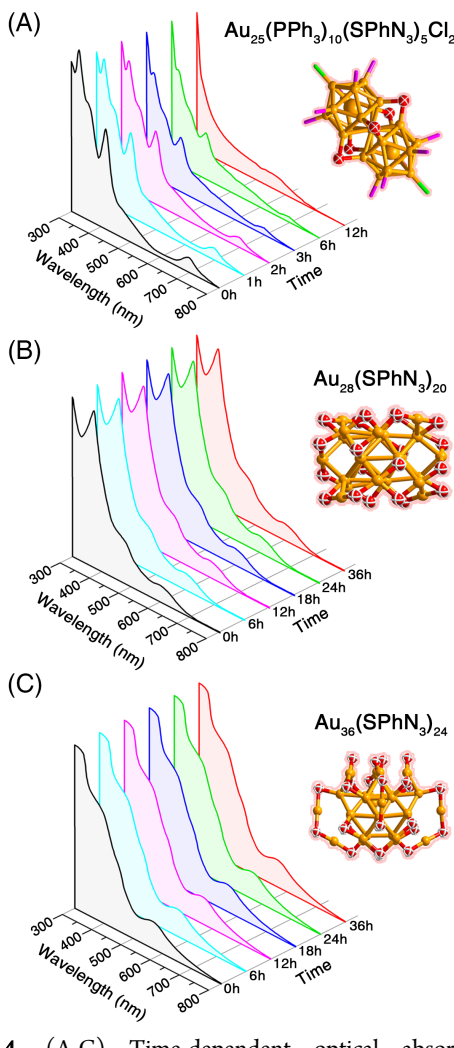


Figure 4. (A-C) Time-dependent optical absorptions of nanoclusters heated at 50 °C. Insets: proposed nanocluster structures.

Although the ligand **5** is unstable due to its spontaneous rearrangement, after its anchorage onto the nanocluster surface, the

electron density associated with the sulfur atom should be greatly reduced, thereby reducing its propensity towards elimination (Figure S3B). To confirm this hypothesis, the thermal stability of the nanoclusters was evaluated by monitoring their optical properties as a function of time at 50 °C. As shown in Figure 4A, characteristic UV-vis absorptions of $\text{Au}_{25}(\text{PPh}_3)_{10}(\text{SPhN}_3)_5\text{Cl}_2$ gradually decreased in intensity after two hours and completely disappeared in approximately 12 hours, indicating degradation. However, the degradation is not due to the spontaneous rearrangement of the -SPhN_3 ligand, as evidenced by the retention of the azide vibration at 2135 cm^{-1} (Figure S10C-D). Instead, the Au_{25} nanocluster itself has degraded into smaller metal complexes, with gold atoms still bound to -SPhN_3 ligands. The majority of the degraded fragments have been identified by ESI-MS (Figure S10F). In contrast, the UV-vis/ESI-MS measurements of $\text{Au}_{28}(\text{SPhN}_3)_{20}$ and $\text{Au}_{36}(\text{SPhN}_3)_{24}$ were essentially identical before and after heating (Figure 4B-C and Figure S11). Of note, when the temperature was further increased from 50 to 100 °C, $\text{Au}_{28}(\text{SPhN}_3)_{20}$ exhibited greater stability than $\text{Au}_{36}(\text{SPhN}_3)_{24}$ (Figure S12). These studies confirmed that the azide ligand **5** was stable once bound to the gold nanoclusters, and therefore supported the downstream functionalization and applications of these azide-nanoclusters.

To confirm that the azide functionalities on the nanocluster remain reactive toward alkynes, we used the $\text{Au}_{28}(\text{SPhN}_3)_{20}$ nanocluster as the substrate to react with a model alkyne ligand. Since Cu(I), often used in conventional click reaction, may cause disruption to the nanocluster,^{78,79} we adopted DBCO-OH as the model alkyne, which does not require Cu(I) and instead relies on strain-promotion to achieve a reasonable reaction rate.^{62,80-82} As shown in Figure 5, the click reaction transformed the clickable nanocluster to $\text{Au}_{28}(\text{SPhN}_3\text{-DBCO-OH})_{20}$. UV-vis spectroscopy showed slight peak broadening after the reaction (Figure 5B). ESI-MS of the reaction product exhibited two well-resolved peaks at 6594.5 and 13056.0 Da (Figure 5C), which can be assigned to $[\text{Au}_{28}(\text{SPhN}_3\text{-DBCO-OH})_{20}\text{Cs}_2]^{2+}$ and $[\text{Au}_{28}(\text{SPhN}_3\text{-DBCO-OH})_{20}\text{Cs}]^+$, respectively. FTIR spectroscopy showed the complete consumption of the azide groups, evidenced by the absence of the typical azide vibration at 2135 cm^{-1} (Figure S13). These results indicate that the azides on the nanocluster surface are chemically accessible for click reaction.

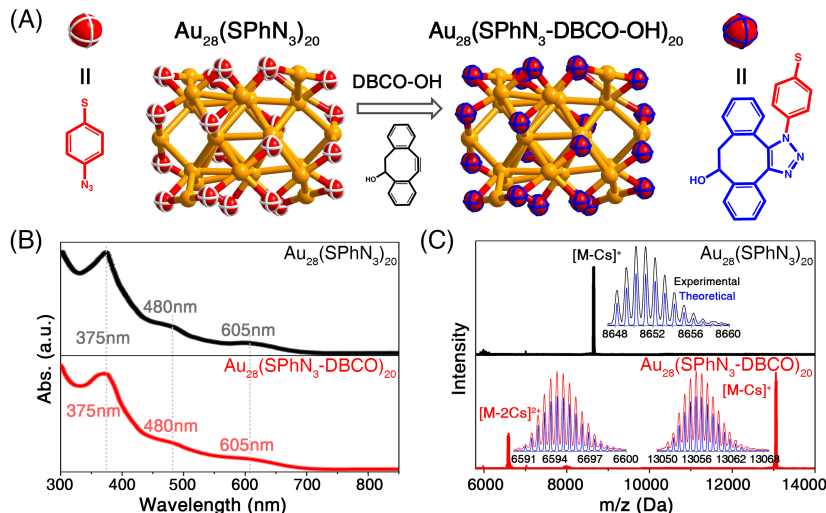


Figure 5. (A) Scheme of model click reaction. (B-C) UV-vis spectroscopy and ESI-MS of the nanocluster substrate and the product.

Summary

We report a ligand exchange process using a rigid azide thiol and pre-made nanocluster precursors to produce clusters with clickable surfaces. Three azide-functionalized nanoclusters, $\text{Au}_{25}(\text{PPh}_3)_{10}(\text{SPhN}_3)_5\text{Cl}_2$, $\text{Au}_{28}(\text{SPhN}_3)_{20}$ and $\text{Au}_{36}(\text{SPhN}_3)_{24}$, are synthesized and characterized. Structures of these nanoclusters are proposed based on reported analogous with corresponding compositions and optical absorptions. While the nanocluster $\text{Au}_{25}(\text{PPh}_3)_{10}(\text{SPhN}_3)_5\text{Cl}_2$ exhibits clickable sites around the “waist” of the rod-shaped particle, both $\text{Au}_{28}(\text{SPhN}_3)_{20}$ and $\text{Au}_{36}(\text{SPhN}_3)_{24}$ clusters display “whole-body” distribution of the azides. The latter two clusters display higher thermal stabilities than $\text{Au}_{25}(\text{PPh}_3)_{10}(\text{SPhN}_3)_5\text{Cl}_2$, making them better candidates for further functionalization and applications. The azide functional groups on the nanocluster surface remain reactive for click chemistry. Overall, this work presents an efficient synthetic approach for preparing nanoclusters with clickable surfaces, which should enable future studies decorating these particles using click chemistry for application-driven purposes.

ASSOCIATED CONTENT

Supporting Information

NMR, TGA, FTIR, EA, and ESI-MS results of nanoclusters. These materials are available free of charge via the Internet at <http://pubs.acs.org>.

AUTHOR INFORMATION

Corresponding Author

*zmq@ahu.edu.cn (M.Z.)

*k.zhang@northeastern.edu (K.Z.)

Author Contributions

[†]X.K. and M.R. contributed equally.

Notes

The authors declare no competing financial interests.

ACKNOWLEDGMENT

M.Z. acknowledges the financial support by NSFC (U1532141, 21631001, 21871001), the Ministry of Education, and the Education Department of Anhui Province. K.Z. acknowledges support from the National Science Foundation (DMR Award Number 2004947).

REFERENCES

- (1) Jin, R.; Zeng, C.; Zhou, M.; Chen, Y. Atomically Precise Colloidal Metal Nanoclusters and Nanoparticles: Fundamentals and Opportunities. *Chem. Rev.* **2016**, *116*, 10346-10413.
- (2) Chakraborty, I.; Pradeep, T. Atomically Precise Clusters of Noble Metals: Emerging Link between Atoms and Nanoparticles. *Chem. Rev.* **2017**, *117*, 8208-8271.
- (3) Cook, A. W.; Hayton, T. W. Case Studies in Nanocluster Synthesis and Characterization: Challenges and Opportunities. *Acc. Chem. Res.* **2018**, *51*, 2456-2464.
- (4) Gan, Z.; Xia, N.; Wu, Z. Discovery, Mechanism, and Application of Antigalvanic Reaction. *Acc. Chem. Res.* **2018**, *51*, 2774-2783.
- (5) Bhattacharai, B.; Zaker, Y.; Atnagulov, A.; Yoon, B.; Landman, U.; Bigioni, T. P. Chemistry and Structure of Silver Molecular Nanoparticles. *Acc. Chem. Res.* **2018**, *51*, 3104-3113.
- (6) Sakthivel, N. A.; Dass, A. Aromatic Thiolate-Protected Series of Gold Nanomolecules and a Contrary Structural Trend in Size Evolution. *Acc. Chem. Res.* **2018**, *51*, 1774-1783.
- (7) Sharma, S.; Chakraborty, K. K.; Saillard, J.-Y.; Liu, C. W. Structurally Precise Dichalcogenolate-Protected Copper and Silver Superatomic Nanoclusters and Their Alloys. *Acc. Chem. Res.* **2018**, *51*, 2475-2483.
- (8) Weerawardene, K. L. D. M.; Häkkinen, H.; Aikens, C. M. Connections Between Theory and Experiment for Gold and Silver Nanoclusters. *Annu. Rev. Phys. Chem.* **2018**, *69*, 205-229.
- (9) Tang, Q.; Hu, G.; Fung, V.; Jiang, D.-e. Insights into Interfaces, Stability, Electronic Properties, and Catalytic Activities of Atomically Precise Metal Nanoclusters from First Principles. *Acc. Chem. Res.* **2018**, *51*, 2793-2802.
- (10) Fang, J.; Zhang, B.; Yao, Q.; Yang, Y.; Xie, J.; Yan, N. Recent Advances in the Synthesis and Catalytic Applications of Ligand-Protected, Atomically Precise Metal Nanoclusters. *Coord. Chem. Rev.* **2016**, *322*, 1-29.
- (11) Nieto-Ortega, B.; Bürgi, T. Vibrational Properties of Thiolate-Protected Gold Nanoclusters. *Acc. Chem. Res.* **2018**, *51*, 2811-2819.
- (12) Agrachev, M.; Ruzzi, M.; Venzo, A.; Maran, F. Nuclear and Electron Magnetic Resonance Spectroscopies of Atomically Precise Gold Nanoclusters. *Acc. Chem. Res.* **2018**, *51*, 44-52.
- (13) Kwak, K.; Lee, D. Electrochemistry of Atomically Precise Metal Nanoclusters. *Acc. Chem. Res.* **2018**, *51*, 12-22.
- (14) Kang, X.; Zhu, M. Metal Nanoclusters Stabilized by Selenol Ligands. *Small* **2019**, *15*, 1902703.
- (15) Yao, Q.; Yuan, X.; Chen, T.; Leong, D. T.; Xie, J. Engineering Functional Metal Materials at the Atomic Level. *Adv. Mater.* **2018**, *30*, 1802751.
- (16) Yan, J.; Teo, B. K.; Zheng, N. Surface Chemistry of Atomically Precise Coinage-Metal Nanoclusters: From Structural Control to Surface Reactivity and Catalysis. *Acc. Chem. Res.* **2018**, *51*, 3084-3093.
- (17) Konishi, K.; Iwasaki, M.; Shichibu, Y. Phosphine-Ligated Gold Clusters with Core+*exo* Geometries: Unique Properties and Interactions at the Ligand-Cluster Interface. *Acc. Chem. Res.* **2018**, *51*, 3125-3133.
- (18) Hossain, S.; Niihori, Y.; Nair, L. V.; Kumar, B.; Kurashige, W.; Negishi, Y. Alloy Clusters: Precise Synthesis and Mixing Effects. *Acc. Chem. Res.* **2018**, *51*, 3114-3124.
- (19) Lei, Z.; Wan, X.-K.; Yuan, S.-F.; Guan, Z.-J.; Wang, Q.-M. Alkynyl Approach toward the Protection of Metal Nanoclusters. *Acc. Chem. Res.* **2018**, *51*, 2465-2474.
- (20) Kang, X.; Zhu, M. Intra-Cluster Growth Meets Inter-Cluster Assembly: The Molecular and Supramolecular Chemistry of Atomically Precise Nanoclusters. *Coord. Chem. Rev.* **2019**, *394*, 1-38.
- (21) Chakraborty, P.; Nag, A.; Chakraborty, A.; Pradeep, T. Approaching Materials with Atomic Precision Using Supramolecular Cluster Assemblies. *Acc. Chem. Res.* **2018**, *51*, 2-11.
- (22) Desiratty, A.; Conn, B. E.; Guo, J.; Yoon, B.; Barnett, R. N.; Monahan, B. M.; Kirschbaum, K.; Griffith, W. P.; Whetten, R. L.; Landman, U.; Bigioni, T. P. Ultrastable Silver Nanoparticles. *Nature* **2013**, *501*, 399-402.
- (23) Conn, B. E.; Atnagulov, A.; Yoon, B.; Barnett, R. N.; Landman, U.; Bigioni, T. P. Confirmation of a de Novo Structure Prediction for an Atomically Precise Monolayer-Coated Silver Nanoparticle. *Sci. Adv.* **2016**, *2*, e1601609.
- (24) Bootharaju, M. S.; Chang, H.; Deng, G.; Malola, S.; Baek, W.; Häkkinen, H.; Zheng, N.; Hyeon, T. $\text{Cd}_{12}\text{Ag}_{36}(\text{SePh})_{36}$: Non-Noble Metal Doped Silver Nanoclusters. *J. Am. Chem. Soc.* **2019**, *141*, 8422-8425.
- (25) Yuan, X.; Sun, C.; Li, X.; Malola, S.; Teo, B. K.; Häkkinen, H.; Zheng, L.-S.; Zheng, N. Combinatorial Identification of Hydrides in a Ligated Ag_{40} Nanocluster with Noncompact Metal Core. *J. Am. Chem. Soc.* **2019**, *141*, 11905-11911.
- (26) Su, Y.-M.; Wang, Z.; Zhuang, G.-L.; Zhao, Q.-Q.; Wang, X.-P.; Tung, C.-H.; Sun, D. Unusual Fcc-Structured Ag_{10} Kernels Trapped in Ag_{70} Nanoclusters. *Chem. Sci.* **2019**, *10*, 564-568.
- (27) Cook, A. W.; Jones, Z. R.; Wu, G.; Scott, S. L.; Hayton, T. W. An Organometallic Cu_{20} Nanocluster: Synthesis, Characterization, Immobilization on Silica, and “Click” Chemistry. *J. Am. Chem. Soc.* **2017**, *140*, 394-400.

(28) Sun, C.; Mammen, N.; Kaappa, S.; Yuan, P.; Deng, G.; Zhao, C.; Yan, J.; Malola, S.; Honkala, K.; Häkkinen, H.; Teo, B. K.; Zheng, N. Atomically Precise, Thiolated Copper-Hydride Nanoclusters as Single-Site Hydrogenation Catalysts for Ketones in Mild Conditions. *ACS Nano* **2019**, *13*, 5975-5986.

(29) Khatun, E.; Chakraborty, P.; Jacob, B. R.; Paramasivam, G.; Bodiuzaaman, M.; Dar, W. A.; Pradeep, T. Intercluster Reactions Resulting in Silver-Rich Trimetallic Nanoclusters. *Chem. Mater.* **2020**, *32*, 611-619.

(30) Baghdasaryan, A.; Besnard, C.; Lawson Daku, L. M.; Delgado, T.; Burgi, T. Thiolato Protected Copper Sulfide Cluster with the Tentative Composition $\text{Cu}_7\text{S}_{15}(2\text{-PET})_{45}$. *Inorg. Chem.* **2020**, *59*, 2200-2208.

(31) Takano, S.; Ito, S.; Tsukuda, T. Efficient and Selective Conversion of Phosphine-Protected $(\text{MAu}_8)^{2+}$ ($\text{M} = \text{Pd, Pt}$) Superatoms to Thiolate-Protected $(\text{MAu}_{12})^{4+}$ or Alkynyl-Protected $(\text{MAu}_{12})^{4+}$ Superatoms via Hydride Doping. *J. Am. Chem. Soc.* **2019**, *141*, 15994-16002.

(32) Fei, W.; Antonello, S.; Dainese, T.; Dolmella, A.; Lahtinen, M.; Rissanen, K.; Venzo, A.; Maran, F. Metal Doping of $\text{Au}_{25}(\text{SR})_{18}$ Clusters: Insights and Hindsights. *J. Am. Chem. Soc.* **2019**, *141*, 16033-16045.

(33) Zhao, Y.; Zhuang, S.; Liao, L.; Wang, C.; Xia, N.; Gan, Z.; Gu, W.; Li, J.; Deng, H.; Wu, Z. A Dual Purpose Strategy to Endow Gold Nanoclusters with Both Catalysis Activity and Water Solubility. *J. Am. Chem. Soc.* **2019**, *142*, 973-977.

(34) Guan, Z.-J.; Hu, F.; Li, J.-J.; Wen, Z.-R.; Lin, Y.-M.; Wang, Q.-M. Isomerization in Alkynyl-Protected Gold Nanoclusters. *J. Am. Chem. Soc.* **2020**, *142*, 2995-3001.

(35) Sakthivel, N. A.; Theivendran, S.; Ganeshraj, V.; Oliver, A. G.; Dass, A. Crystal Structure of Faradaurate-279: $\text{Au}_{279}(\text{SPh}-t\text{Bu})_{84}$ Plasmonic Nanocrystal Molecules. *J. Am. Chem. Soc.* **2017**, *139*, 15450-15459.

(36) Zhu, Y.; Wang, H.; Wan, K.; Guo, J.; He, C.; Yu, Y.; Zhao, L.; Zhang, Y.; Lv, J.; Shi, L.; Jin, R.; Zhang, X.; Shi, X.; Tang, Z. Enantioseparation of $\text{Au}_{20}(\text{PPh}_3)_4\text{Cl}_4$ Clusters with Intrinsically Chiral Cores. *Angew. Chem. Int. Ed.* **2018**, *57*, 9059-9063.

(37) Sugiuchi, M.; Shichibu, Y.; Konishi, K. An Inherently Chiral Au_{24} Framework with Double-Helical Hexagold Strands. *Angew. Chem. Int. Ed.* **2018**, *57*, 7855-7859.

(38) Hosier, C. A.; Ackerson, C. J. Regiochemistry of Thiolate for Selenolate Ligand Exchange on Gold Clusters. *J. Am. Chem. Soc.* **2018**, *141*, 309-314.

(39) Cirri, A.; Morales Hernández, H.; Kmiotek, C.; Johnson, C. J. Systematically Tuning the Electronic Structure of Gold Nanoclusters through Ligand Derivatization. *Angew. Chem. Int. Ed.* **2019**, *58*, 13818-13822.

(40) Yang, D.; Pei, W.; Zhou, S.; Zhao, J.; Ding, W.; Zhu, Y. Controllable Conversion of CO_2 on Non-Metallic Gold Clusters. *Angew. Chem. Int. Ed.* **2020**, *59*, 1919-1924.

(41) Huang, R.-W.; Wei, Y.-S.; Dong, X.-Y.; Wu, X.-H.; Du, C.-X.; Zang, S.-Q.; Mak, T. C. W. Hypersensitive Dual-Function Luminescence Switching of a Silver-Chalcogenolate Cluster-Based Metal-Organic Framework. *Nat. Chem.* **2017**, *9*, 689-697.

(42) Alhilaly, M. J.; Huang, R.-W.; Naphade, R.; Alamer, B.; Hedhili, M. N.; Emwas, A.-H.; Maity, P.; Yin, J.; Shkurenko, A.; Mohammed, O. F.; Eddaoudi, M.; Bakr, O. M. Assembly of Atomically Precise Silver Nanoclusters into Nanocluster-Based Frameworks. *J. Am. Chem. Soc.* **2019**, *141*, 9585-9592.

(43) Wang, Z.; Su, H.-F.; Gong, Y.-W.; Qu, Q.-P.; Bi, Y.-F.; Tung, C.-H.; Sun, D.; Zheng, L.-S. A hierarchically Assembled 88-Nuclei Silver-Thiacalix[4]arene nanocluster. *Nat. Commun.* **2020**, *11*, 308.

(44) Zhuang, S.; Chen, D.; Liao, L.; Zhao, Y.; Xia, N.; Zhang, W.; Wang, C.; Yang, J.; Wu, Z. Hard-Sphere Random Close-Packed $\text{Au}_4\text{Cd}_2(\text{TBBT})_{31}$ Nanoclusters with a Faradaic Efficiency of Up to 96% for Electrocatalytic CO_2 Reduction to CO. *Angew. Chem. Int. Ed.* **2020**, *59*, 3073-3077.

(45) Qu, M.; Zhang, F.-Q.; Wang, D.-H.; Li, H.; Hou, J.-J.; Zhang, X.-M. Observation of non-FCC Copper in Alkynyl-Protected Cu_{53} Nanoclusters. *Angew. Chem. Int. Ed.* **2020**, *59*, 6507-6512.

(46) Narouz, M. R.; Osten, K. M.; Unsworth, P. J.; Man, R. W. Y.; Salorinne, K.; Takano, S.; Tomihara, R.; Kaappa, S.; Malola, S.; Dinh, C.-T.; Padmos, J. D.; Ayoo, K.; Garrett, P. J.; Nambo, M.; Horton, J. H.; Sargent, E. H.; Häkkinen, H.; Tsukuda, T.; Cradden, C. M. N-heterocyclic Carbene-Functionalized Magic-Number Gold Nanoclusters. *Nat. Chem.* **2019**, *11*, 419-425.

(47) Shen, H.; Deng, G.; Kaappa, S.; Tan, T.; Han, Y.-Z.; Malola, S.; Lin, S.-C.; Teo, B. K.; Häkkinen, H.; Zheng, N. Highly Robust but Surface-Active: An N-Heterocyclic Carbene-Stabilized Au_{25} Nanocluster. *Angew. Chem. Int. Ed.* **2019**, *58*, 17731-17735.

(48) Lei, Z.; Pei, X.-L.; Guan, Z.-J.; Wang, Q.-M. Full Protection of Intensely Luminescent Gold(I)-Silver(I) Cluster by Phosphine Ligands and Inorganic Anions. *Angew. Chem. Int. Ed.* **2017**, *56*, 7117-7120.

(49) Wu, Z.; Jin, R. On the Ligand's Role in the Fluorescence of Gold Nanoclusters. *Nano Lett.* **2010**, *10*, 2568-2573.

(50) Zeng, C.; Chen, Y.; Das, A.; Jin, R. Transformation Chemistry of Gold Nanoclusters: From One Stable Size to Another. *J. Phys. Chem. Lett.* **2015**, *6*, 2976-2986.

(51) Kang, X.; Zhu, M. Transformation of Atomically Precise Nanoclusters by Ligand-Exchange. *Chem. Mater.* **2019**, *31*, 9939-9969.

(52) Bootharaju, M. S.; Joshi, C. P.; Alhilaly, M. J.; Bakr, O. M. Switching a Nanocluster Core from Hollow to Nonhollow. *Chem. Mater.* **2016**, *28*, 3292-3297.

(53) Lin, Y.; Charchar, P.; Christofferson, A. J.; Thomas, M. R.; Todorova, N.; Mazo, M. M.; Chen, Q.; Douth, J.; Richardson, R.; Yarovsky, I.; Stevens, M. M. Surface Dynamics and Ligand-Core Interactions of Quantum Sized Photoluminescent Gold Nanoclusters. *J. Am. Chem. Soc.* **2018**, *140*, 18217.

(54) Li, J.; Nasaruddin, R. R.; Feng, Y.; Yang, J.; Yan, N.; Xie, J. Tuning the Accessibility and Activity of $\text{Au}_{25}(\text{SR})_{18}$ Nanocluster Catalysts through Ligand Engineering. *Chem. Eur. J.* **2016**, *22*, 14816-14820.

(55) Li, G.; Abroshan, H.; Liu, C.; Zhuo, S.; Li, Z.; Xie, Y.; Kim, H. J.; Rosi, N. L.; Jin, R. Tailoring the Electronic and Catalytic Properties of Au_{25} Nanoclusters via Ligand Engineering. *ACS Nano* **2016**, *10*, 7998-8005.

(56) Li, S.; Du, X.-S.; Li, B.; Wang, J.-Y.; Li, G.-P.; Gao, G.-G.; Zang, S.-Q. Atom-Precise Modification of Silver(I) Thiolate Cluster by Shell Ligand Substitution: A New Approach to Generation of Cluster Functionality and Chirality. *J. Am. Chem. Soc.* **2018**, *140*, 594-597.

(57) Yang, H.; Wang, Y.; Lei, J.; Shi, L.; Wu, X.; Makinen, V.; Lin, S.; Tang, Z.; He, J.; Häkkinen, H.; Zheng, L.; Zheng, N. Ligand-Stabilized $\text{Au}_{13}\text{Cu}_x$ ($x = 2, 4, 8$) Bimetallic Nanoclusters: Ligand Engineering to Control the Exposure of Metal Sites. *J. Am. Chem. Soc.* **2013**, *135*, 9568-9571.

(58) Kang, X.; Huang, L.; Liu, W.; Xiong, L.; Pei, Y.; Sun, Z.; Wang, S.; Wei, S.; Zhu, M. Reversible Nanocluster Structure Transformation between Face-Centered Cubic and Icosahedral Isomers. *Chem. Sci.* **2019**, *10*, 8685-8693.

(59) Chen, Y.; Liu, C.; Tang, Q.; Zeng, C.; Higaki, T.; Das, A.; Jiang, D.-E.; Rosi, N. L.; Jin, R. Isomerism in $\text{Au}_{25}(\text{SR})_{20}$ Nanocluster and Stable Structures. *J. Am. Chem. Soc.* **2016**, *138*, 1482-1485.

(60) Higaki, T.; Liu, C.; Zhou, M.; Luo, T.-Y.; Rosi, N. L.; Jin, R. Tailoring the Structure of 58-Electron Gold Nanoclusters: $\text{Au}_{103}\text{S}_2(\text{SNap})_{41}$ and Its Implications. *J. Am. Chem. Soc.* **2017**, *139*, 9994-10001.

(61) Cao, M.; Pang, R.; Wang, Q.-Y.; Han, Z.; Wang, Z.-Y.; Dong, X.-Y.; Li, S.-F.; Zang, S.-Q.; Mak, T. C. W. M. Porphyrinic Silver Cluster Assembled Material for Simultaneous Capture and Photocatalysis of Mustard-Gas Simulant. *J. Am. Chem. Soc.* **2019**, *141*, 14505-14509.

(62) Gunawardene, P. N.; Corrigan, J. F.; Workentin, M. S. Golden Opportunity: A Clickable Azide-Functionalized $[\text{Au}_{25}(\text{SR})_{18}]$ Nanocluster Platform for Interfacial Surface Modifications. *J. Am. Chem. Soc.* **2019**, *141*, 11781-11785.

(63) Aldeek, F.; Muhammed, M. A. H.; Palui, G.; Zhan, N.; Matoussi, H. Growth of Highly Fluorescent Polyethylene Glycol- and Zwitterion-Functionalized Gold Nanoclusters. *ACS Nano* **2013**, *7*, 2509-2521.

(64) Palui, G.; Aldeek, F.; Wang, W.; Matoussi, H. Strategies for Interfacing Inorganic Nanocrystals with Biological Systems based on Polymer-Coating. *Chem. Soc. Rev.* **2015**, *44*, 193-227.

(65) Mishra, D.; Wang, S.; Jin, Z.; Xin, Y.; Lochner, E.; Matoussi, H. Highly Fluorescent Hybrid Au/Ag Nanoclusters Stabilized with Poly(ethylene glycol)- and Zwitterion-Modified Thiolate Ligands. *Phys. Chem. Chem. Phys.* **2019**, *21*, 21317-21328.

(66) McKenzie, L. C.; Zaikova, T. O.; Hutchison, J. E. Structurally Similar Triphenylphosphine-Stabilized Undecagolds, $\text{Au}_{11}(\text{PPh}_3)_7\text{Cl}_3$ and

[Au₁₁(PPh₃)₈Cl₂]Cl, Exhibit Distinct Ligand Exchange Pathways with Glutathione. *J. Am. Chem. Soc.* **2014**, *136*, 13426-13435.

(67) Das, A.; Li, T.; Nobusada, K.; Zeng, C.; Rosi, N. L.; Jin, R. Nonsuperatomic [Au₂₃(SC₆H₁₁)₁₆]⁺ Nanocluster Featuring Bipyramidal Au₁₅ Kernel and Trimeric Au₃(SR)₄ Motif. *J. Am. Chem. Soc.* **2013**, *135*, 18264-18267.

(68) Zhu, M.; Lanni, E.; Garg, N.; Bier, M. E.; Jin, R. Kinetically Controlled, High-Yield Synthesis of Au₂₅ Clusters. *J. Am. Chem. Soc.* **2008**, *130*, 1138-1139.

(69) Crasto, D.; Dass, A. Green Gold: Au₃₀(S-t-C₄H₉)₁₈ Molecules. *J. Phys. Chem. C* **2013**, *117*, 22094-22097.

(70) Qian, H.; Eckenhoff, W. T.; Zhu, Y.; Pintauer, T.; Jin, R. Total Structure Determination of Thiolate-Protected Au₃₈ Nanoparticles. *J. Am. Chem. Soc.* **2010**, *132*, 8280-8281.

(71) Barral, K.; Moorhouse, A. D.; Moses, J. E. Efficient Conversion of Aromatic Amines into Azides: A One-Pot Synthesis of Triazole Linkages. *Org. Lett.* **2007**, *9*, 1809-1811.

(72) Shichibu, Y.; Negishi, Y.; Watanabe, T.; Chaki, N. K.; Kawaguchi, H.; Tsukuda, T. Biicosahedral Gold Clusters [Au₂₅(PPh₃)₁₀(SC_nH_{2n+1})₅Cl₂]²⁺ (*n* = 2-18): A Stepping Stone to Cluster-Assembled Materials. *J. Phys. Chem. C* **2007**, *111*, 7845-7847.

(73) Zeng, C.; Li, T.; Das, A.; Rosi, N. L.; Jin, R. Chiral Structure of Thiolate-Protected 28-Gold-Atom Nanocluster Determined by X - ray Crystallography. *J. Am. Chem. Soc.* **2013**, *135*, 10011-10013.

(74) Higaki, T.; Liu, C.; Chen, Y.; Zhao, S.; Zeng, C.; Jin, R.; Wang, S.; Rosi, N. L.; Jin, R. Oxidation-Induced Transformation of Eight-Electron Gold Nanoclusters: [Au₂₃(SR)₁₆]⁺ to [Au₂₈(SR)₂₀]⁰. *J. Phys. Chem. Lett.* **2017**, *8*, 866-870.

(75) Zeng, C.; Qian, H.; Li, T.; Li, G.; Rosi, N. L.; Yoon, B.; Barnett, R. N.; Whetten, R. L.; Landman, U.; Jin, R. Total Structure and Electronic Properties of the Gold Nanocrystal Au₃₆(SR)₂₄. *Angew. Chem. Int. Ed.* **2012**, *51*, 13114-13118.

(76) Zeng, C.; Liu, C.; Pei, Y.; Jin, R. Thiol Ligand-Induced Transformation of Au₃₈(SC₂H₄Ph)₂₄ to Au₃₆(SPh-t-Bu)₂₄. *ACS Nano* **2013**, *7*, 6138-6145.

(77) Dass, A.; Jones, T. C.; Theivendran, S.; Sementa, L.; Fortunelli, A. Core Size Interconversions of Au₃₀(S-t-Bu)₁₈ and Au₃₆(SPhX)₂₄. *J. Phys. Chem. C* **2017**, *121*, 14914-14919.

(78) Kang, X.; Wei, X.; Jin, S.; Yuan, Q.; Luan, X.; Pei, Y.; Wang, S.; Zhu, M.; Jin, R. Rational Construction of a Library of M₂₉ Nanoclusters from Monometallic to Tetrametallic. *Proc. Natl. Acad. Sci. USA* **2019**, *116*, 18834-18840.

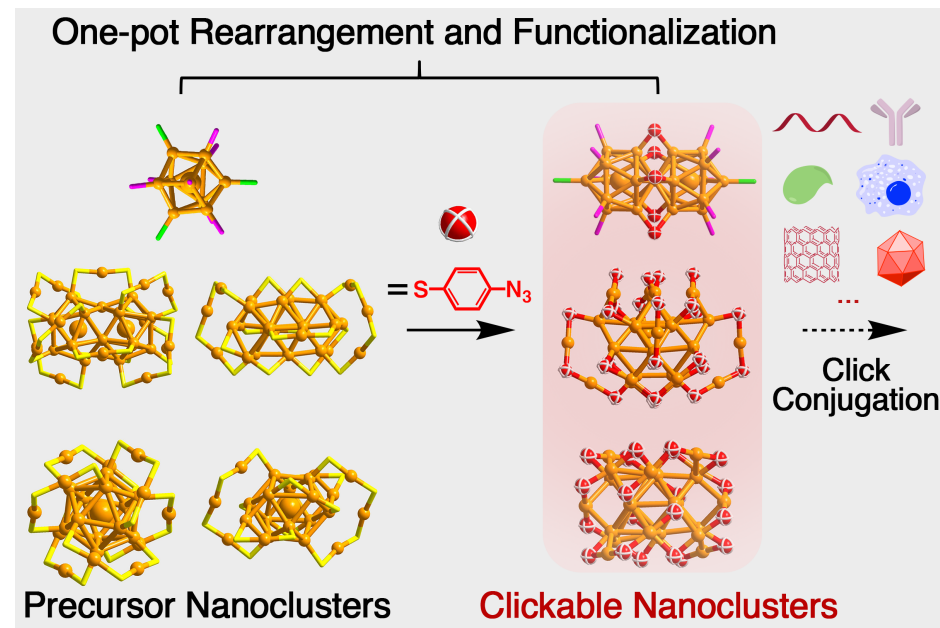
(79) Kang, X.; Abroshan, H.; Wang, S.; Zhu, M. Free Valence Electron Centralization Strategy for Preparing Ultrastable Nanoclusters and Their Catalytic Application. *Inorg. Chem.* **2019**, *58*, 11000-11009.

(80) Gobbo, P.; Novoa, S.; Biesinger, M. C.; Workentin, M. S. Interfacial strain-promoted alkyne-azide cycloaddition (I-SPAAC) for the synthesis of nanomaterial hybrids. *Chem. Commun.* **2013**, *49*, 3982-3984.

(81) Wang, X.; Gobbo, P.; Suchy, M.; Workentin, M. S.; Hudson, R. H. E. Peptide-decorated gold nanoparticles via strain-promoted azidealkyne cycloaddition and post assembly deprotection. *RSC Adv.* **2014**, *4*, 43087-43091.

(82) Agard, N. J.; Prescher, J. A.; Bertozzi, C. R. A strain-promoted [3 + 2] azide-alkyne cycloaddition for covalent modification of biomolecules in living systems. *J. Am. Chem. Soc.* **2004**, *126*, 15046-15047.

Table of Contents



Supporting Information:

Azide-Functionalized Nanoclusters via Ligand-Induced Rearrangement

Xi Kang,^{1,2,§} Mengqi Ren,^{1,§} Manzhou Zhu,^{2,*} Ke Zhang^{1,*}

¹Department of Chemistry and Chemical Biology, Northeastern University, Boston, MA 02115, USA.

²Department of Chemistry and Centre for Atomic Engineering of Advanced Materials, Anhui University, Hefei, Anhui 230601, P. R. China.

[§]X.K. and M.R. contributed equally.

*E-mails of corresponding authors: zmz@ahu.edu.cn (M.Z.); k.zhang@northeastern.edu (K.Z.)

Notes: The authors declare no competing financial interest.

Content:

Materials and Methods

Table S1. EA of azide-functionalized nanoclusters.

Figure S1. NMR of S-(4-nitrophenyl) ethanethioate.

Figure S2. NMR of S-(4-azidophenyl) ethanethioate.

Figure S3. Possible spontaneous rearrangement of 4-azidobenzenethiol.

Figure S4. TGA of $[\text{Au}_{25}(\text{PPh}_3)_{10}(\text{SPhN}_3)_5\text{Cl}_2]\text{Cl}_2$.

Figure S5. FTIR of $[\text{Au}_{25}(\text{PPh}_3)_{10}(\text{SPhN}_3)_5\text{Cl}_2]\text{Cl}_2$.

Figure S6. TGA of $\text{Au}_{28}(\text{SPhN}_3)_{20}$.

Figure S7. FTIR of $\text{Au}_{28}(\text{SPhN}_3)_{20}$.

Figure S8. TGA of $\text{Au}_{36}(\text{SPhN}_3)_{24}$.

Figure S9. FTIR of $\text{Au}_{36}(\text{SPhN}_3)_{24}$.

Figure S10. Characterization of $\text{Au}_{25}(\text{PPh}_3)_{10}(\text{SPhN}_3)_5\text{Cl}_2$ and its decomposition products.

Figure S11. ESI-MS of $\text{Au}_{28}(\text{SPhN}_3)_{20}$ and $\text{Au}_{36}(\text{SPhN}_3)_{24}$ before and after the heat treatment.

Figure S12. Thermal stability studies for $\text{Au}_{28}(\text{SPhN}_3)_{20}$ and $\text{Au}_{36}(\text{SPhN}_3)_{24}$.

Figure S13. FTIR of $\text{Au}_{28}(\text{SPhN}_3)_{20}$ and $\text{Au}_{28}(\text{SPhN}_3\text{-DBCO-OH})_{20}$.

Materials and Methods

Chemicals. All reagents were purchased from Sigma-Aldrich or Fisher Scientific and used without further purification: tetrachloroauric (III) acid ($\text{HAuCl}_4 \bullet 3\text{H}_2\text{O}$, 99.99% metals basis), triphenylphosphine (PPh_3 , 99%), cyclohexanethiol ($\text{HS-}c\text{-C}_6\text{H}_11\text{SH}$, 95%), 2-phenylethanethiol ($\text{HSC}_2\text{H}_4\text{Ph}$, 97%), tert-butylthiol ($\text{HS-}t\text{-C}_4\text{H}_9$, 95%), sodium borohydride (NaBH_4 , 98%), tetraoctylammonium bromide (TOAB, 99%), 4-nitrobenzenethiol ($\text{NO}_2\text{-Ph-SH}$, 95%), acetyl chloride (CH_3COCl , 98%), trimethylamine (NET_3 , 99%), anhydrous tin(II) chloride (SnCl_2 , 99%), tert-butyl nitrite ($t\text{BuO-NO}$, 90%), trimethylsilyl azide (TMS-N₃, 95%), 5-hydroxy-1,2:5,6-dibenzocyclooct-7-yne (DBCO-OH, 97%), anhydrous dichloromethane (CH_2Cl_2 , HPLC, Sigma-Aldrich), methanol (CH_3OH , HPLC, Sigma-Aldrich), anhydrous acetonitrile (CH_3CN), hexane ($n\text{-C}_6\text{H}_{12}$, HPLC, Sigma-Aldrich), toluene (Ph-CH_3 , HPLC, Sigma-Aldrich).

Characterizations. The UV-vis absorption spectra of nanoclusters were recorded using an Agilent 8453 diode array spectrometer. Electrospray ionization mass spectrometry (ESI-MS) measurements were performed by MicrOTOF-QIII high-resolution mass spectrometer. The sample was directly infused into the chamber at 5 $\mu\text{L}/\text{min}$. For preparing the ESI samples, nanoclusters were dissolved in CH_2Cl_2 (1 mg/mL) and diluted ($v/v = 1:2$) by CH_3OH . Thermogravimetric analysis (TGA) was carried out on a thermogravimetric analyzer (DTG-60H, Shimadzu Instruments, Inc.). 10 mg of each nanocluster was used for collecting the corresponding TGA data. Nuclear Magnetic Resonance (NMR) measurements including ¹H NMR and ¹³C NMR were carried out on 500 MHz Varian Inova. Fourier-transform infrared (FTIR) measurements were recorded on BRUKER ALPHA FT-IR Spectrometer. Elemental Analysis (EA) measurements were performed on EuroVector S.p.A. - EuroEA3000 CHNS-O Analyzer.

Table S1. Elemental analysis (C, H, N, and S contents) of azide-functionalized nanoclusters.

$[\text{Au}_{25}(\text{PPh}_3)_{10}(\text{SPhN}_3)_5\text{Cl}_2]\text{Cl}_2$	C wt%	H wt%	N wt%	S wt%
Experimental	19.95%	1.99%	2.45%	2.06%
Theoretical	18.57%	2.02%	2.50%	1.91%

$\text{Au}_{28}(\text{SPhN}_3)_{20}$	C wt%	H wt%	N wt%	S wt%
Experimental	16.94%	1.05%	9.35%	7.22%
Theoretical	16.94%	0.94%	9.88%	7.53%

$\text{Au}_{36}(\text{SPhN}_3)_{24}$	C wt%	H wt%	N wt%	S wt%
Experimental	16.15%	1.08%	9.05%	6.98%
Theoretical	16.15%	0.90%	9.42%	7.18%

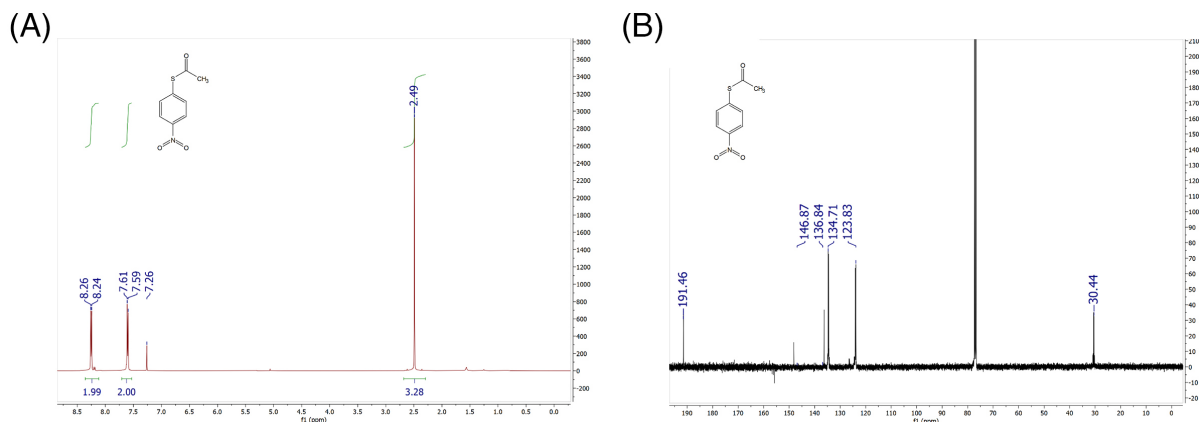


Figure S1. (A) ^1H NMR and (B) ^{13}C NMR spectra of S-(4-nitrophenyl) ethanethioate.

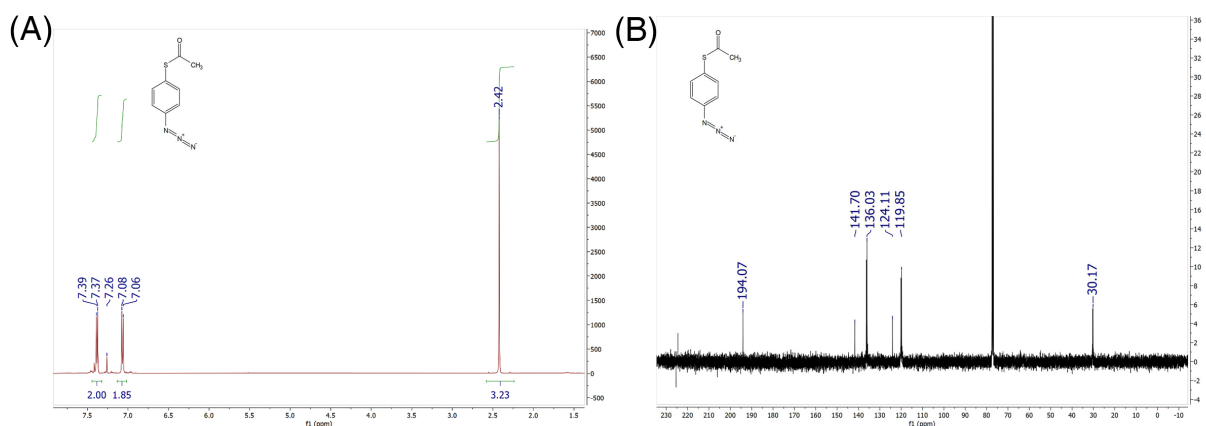


Figure S2. (A) ^1H NMR and (B) ^{13}C NMR spectra of S-(4-azidophenyl) ethanethioate.

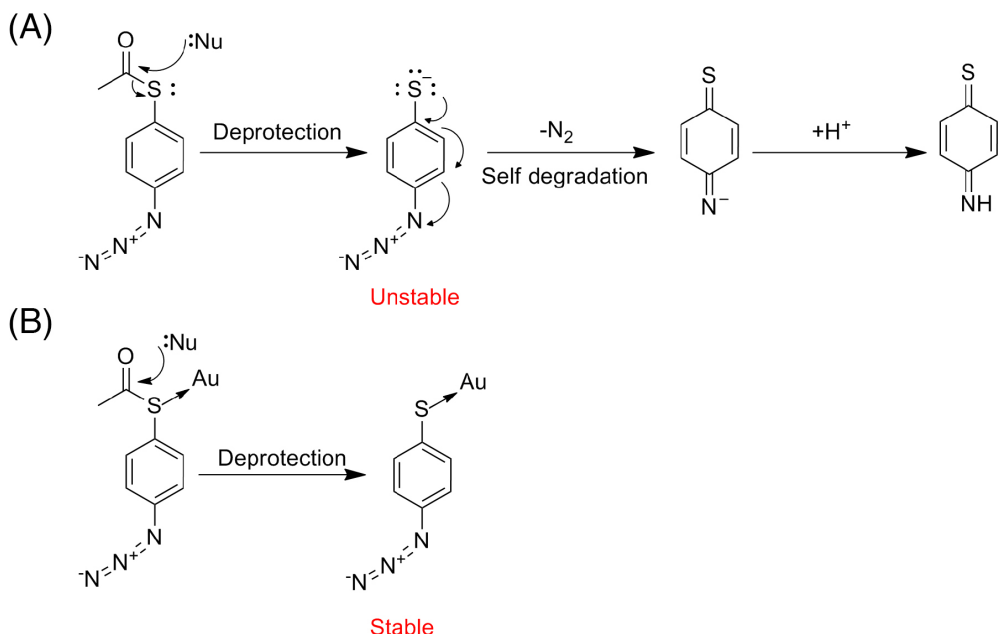


Figure S3. (A) A possible pathway for the spontaneous decomposition of 4-azidobenzenethiol. (B) Binding to Au atom reduces the electron density of S, thus making the ligand more stable.

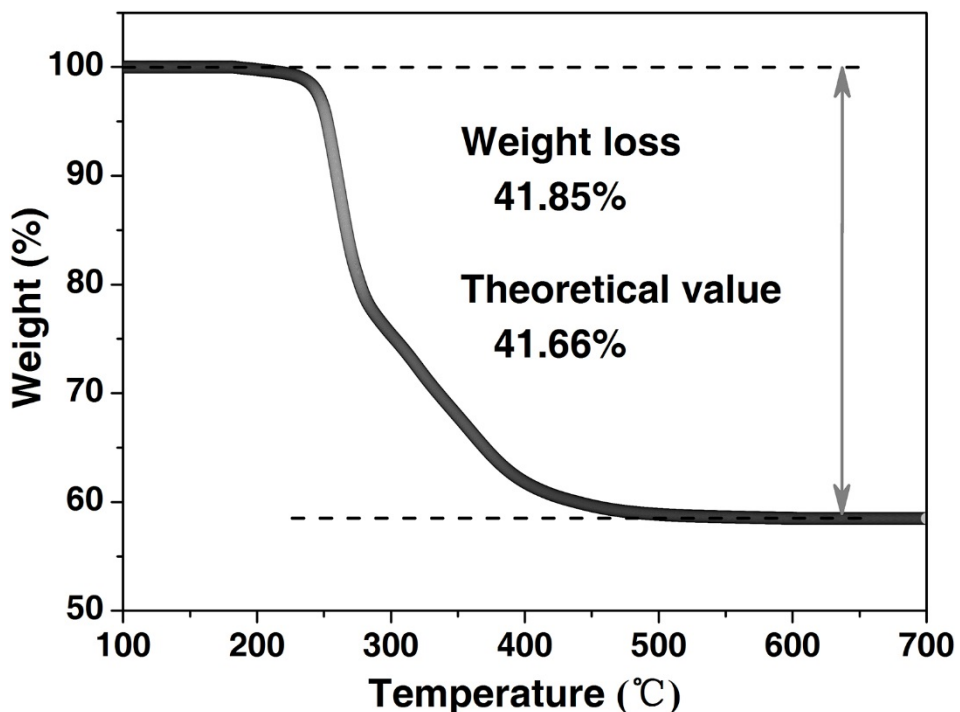


Figure S4. TGA of $[\text{Au}_{25}(\text{PPh}_3)_{10}(\text{SPhN}_3)_5\text{Cl}_2]\text{Cl}_2$. The weight loss of 41.85% is consistent with the calculated loss (41.66%) of PPh_3 , SPhN_3 and Cl ligands and Cl counterions in the $[\text{Au}_{25}(\text{PPh}_3)_{10}(\text{SPhN}_3)_5\text{Cl}_2]\text{Cl}_2$ nanocluster.

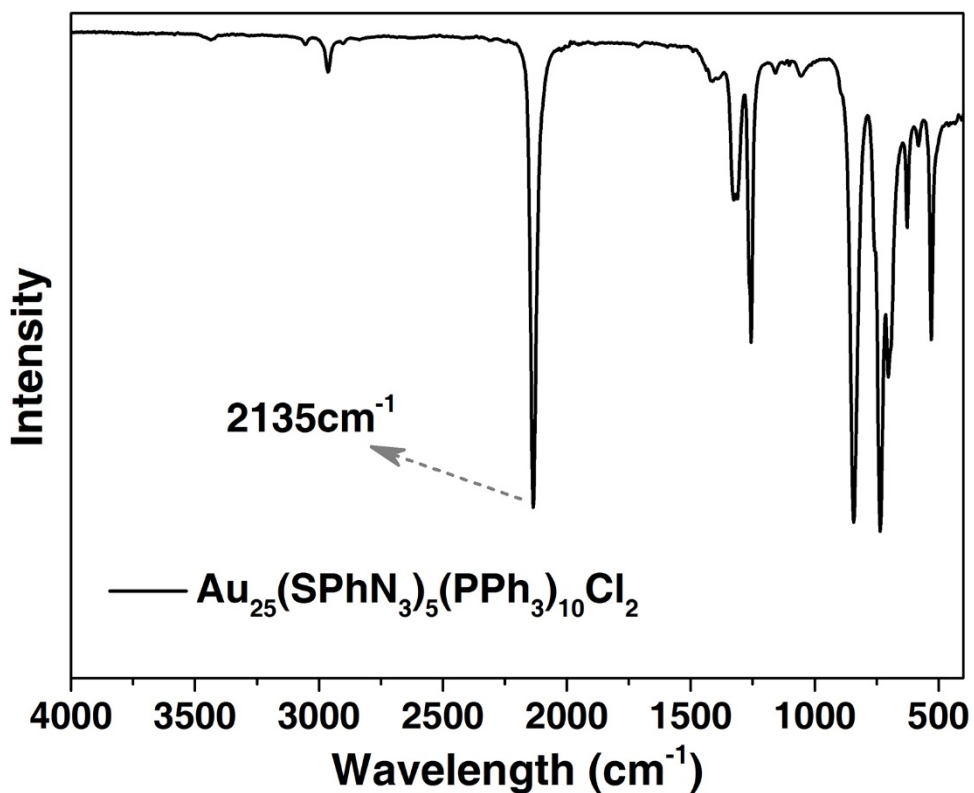


Figure S5. FTIR spectrum of $[\text{Au}_{25}(\text{PPh}_3)_{10}(\text{SPhN}_3)_5\text{Cl}_2]\text{Cl}_2$, showing characteristic azide vibration.

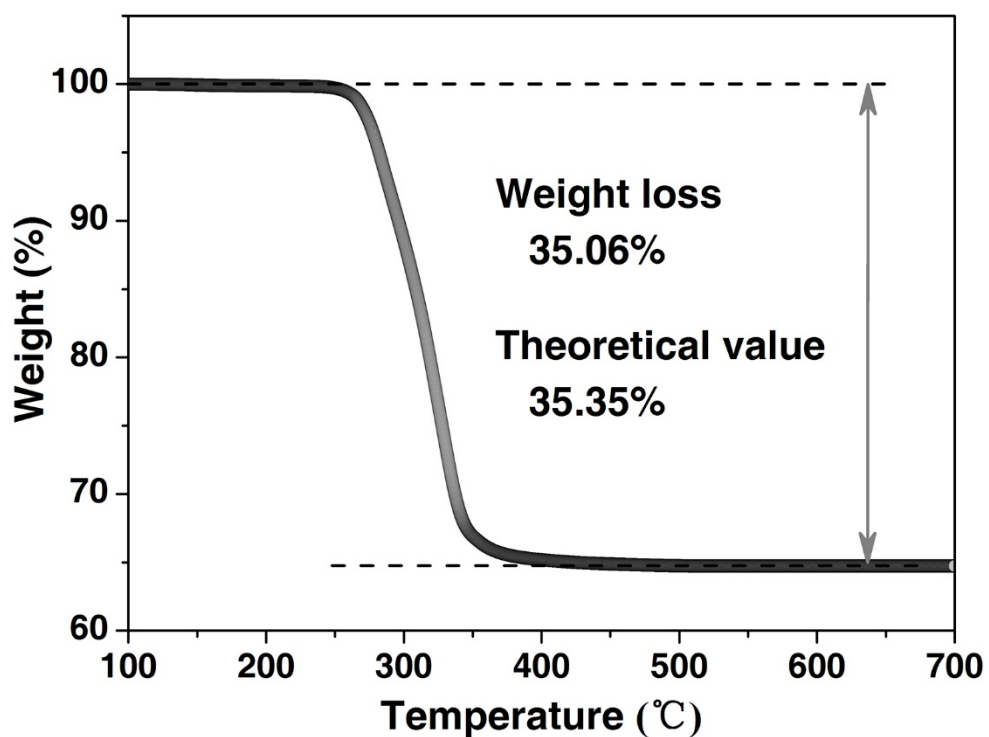


Figure S6. TGA of $\text{Au}_{28}(\text{SPhN}_3)_{20}$. The weight loss of 35.06% is consistent with the calculated loss (35.35%) of SPhN_3 ligands in the $\text{Au}_{28}(\text{SPhN}_3)_{20}$ nanocluster.

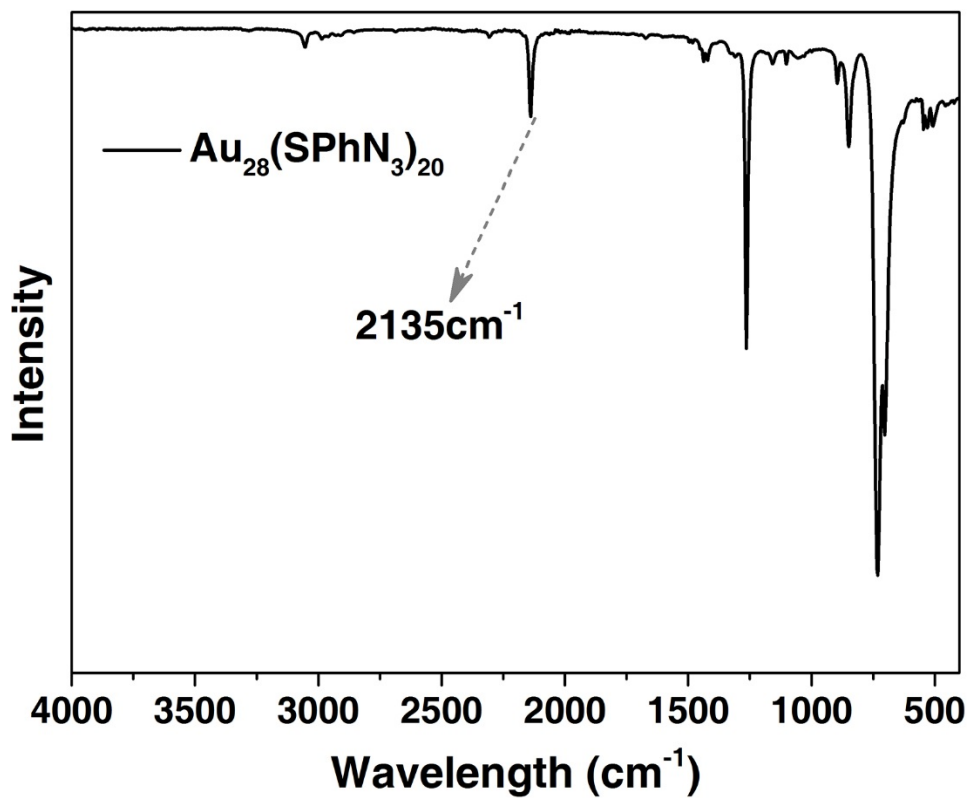


Figure S7. FTIR spectrum of $\text{Au}_{28}(\text{SPhN}_3)_{20}$, showing characteristic azide vibration.

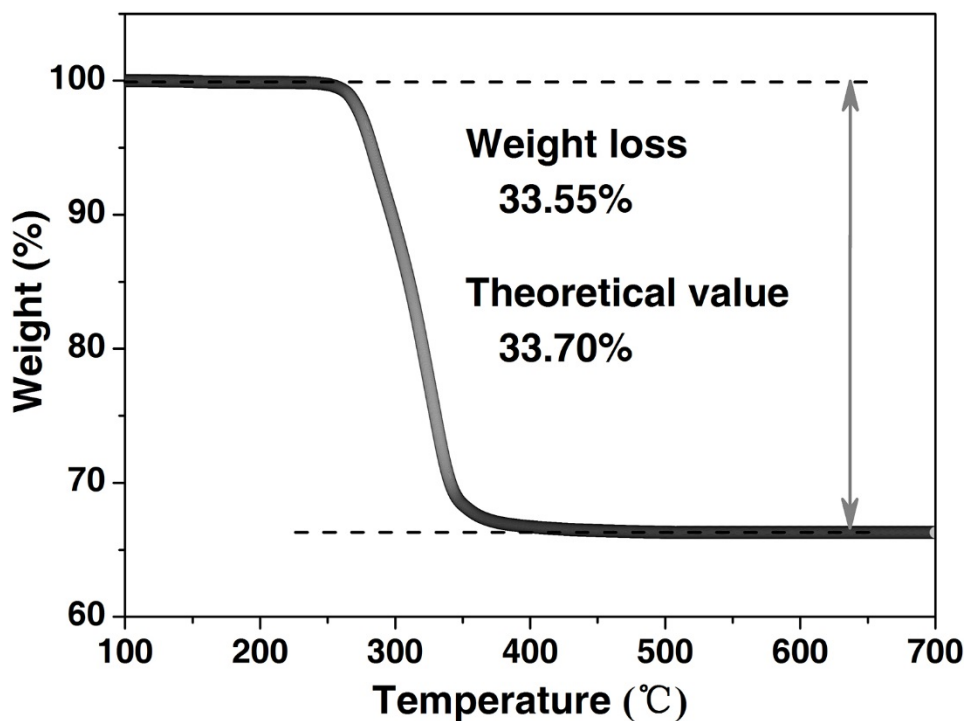


Figure S8. TGA result of $\text{Au}_{36}(\text{SPhN}_3)_{24}$. The weight loss of 33.55% was consistent with the calculated loss (33.70%) of SPhN_3 ligands in the $\text{Au}_{36}(\text{SPhN}_3)_{24}$ nanocluster.

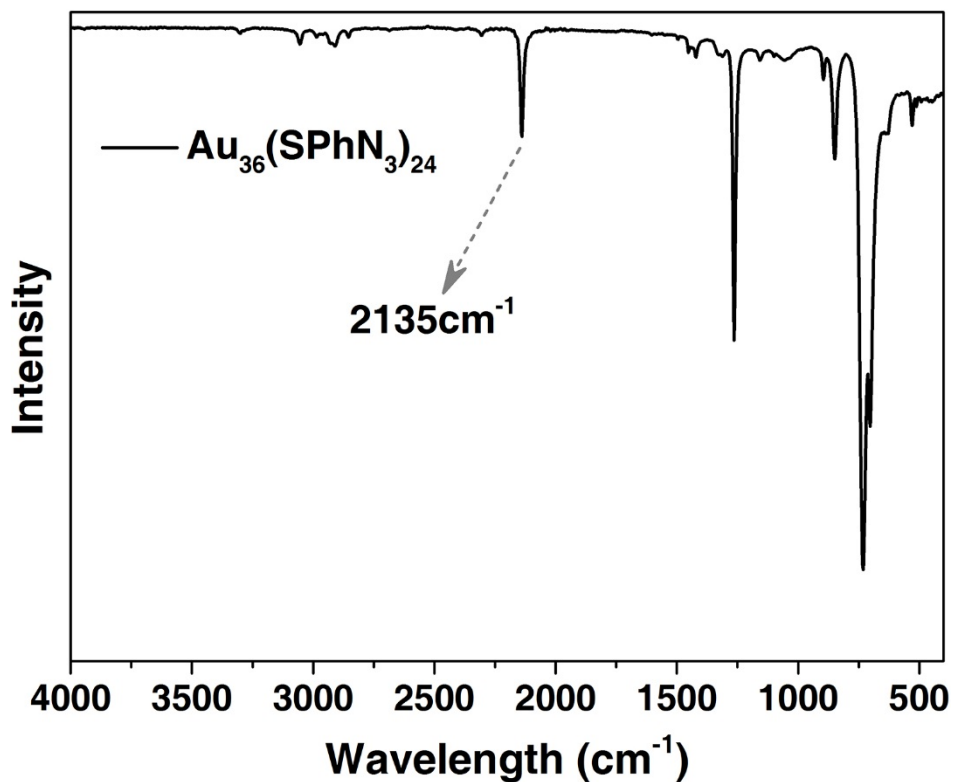


Figure S9. FTIR spectrum of $\text{Au}_{36}(\text{SPhN}_3)_{24}$, showing characteristic azide vibration.

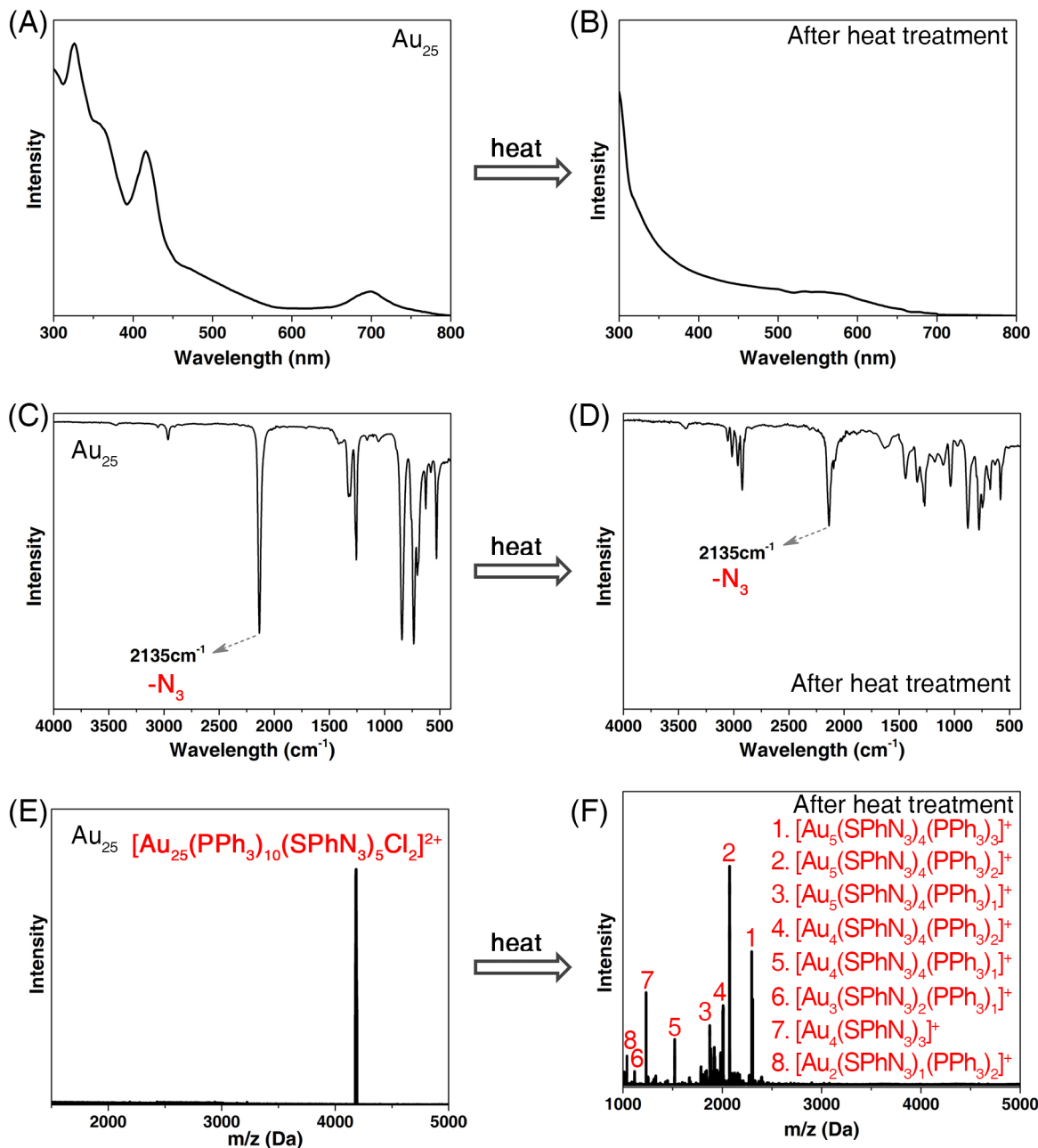


Figure S10. UV-vis, FTIR, and ESI-MS spectra of the nanocluster $\text{Au}_{25}(\text{PPh}_3)_{10}(\text{SPhN}_3)_5\text{Cl}_2$ in CH_2Cl_2 before and after heat treatment at 50 °C for 12 hours. Loss of the characteristic optical absorptions and the mass signal of $[\text{Au}_{25}(\text{PPh}_3)_{10}(\text{SPhN}_3)_5\text{Cl}_2]^{2+}$ is observed. However, the azide vibration remains, suggesting that the degradation is not due to ligand loss. Instead, the S-PhN₃ ligands are still anchored to the Au atoms, which are in the form of metal nanoclusters and metal complexes.

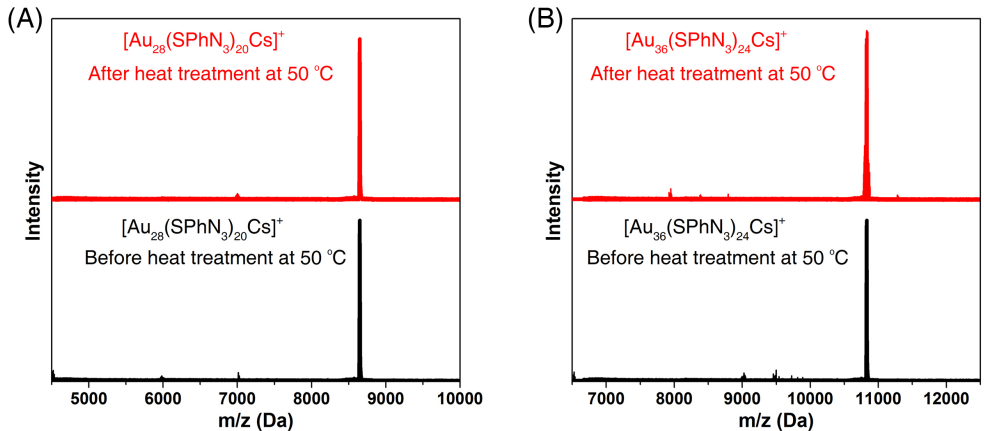


Figure S11. ESI-MS of (A) $\text{Au}_{28}(\text{SPhN}_3)_{20}$ and (B) $\text{Au}_{36}(\text{SPhN}_3)_{24}$ before and after heat treatment.

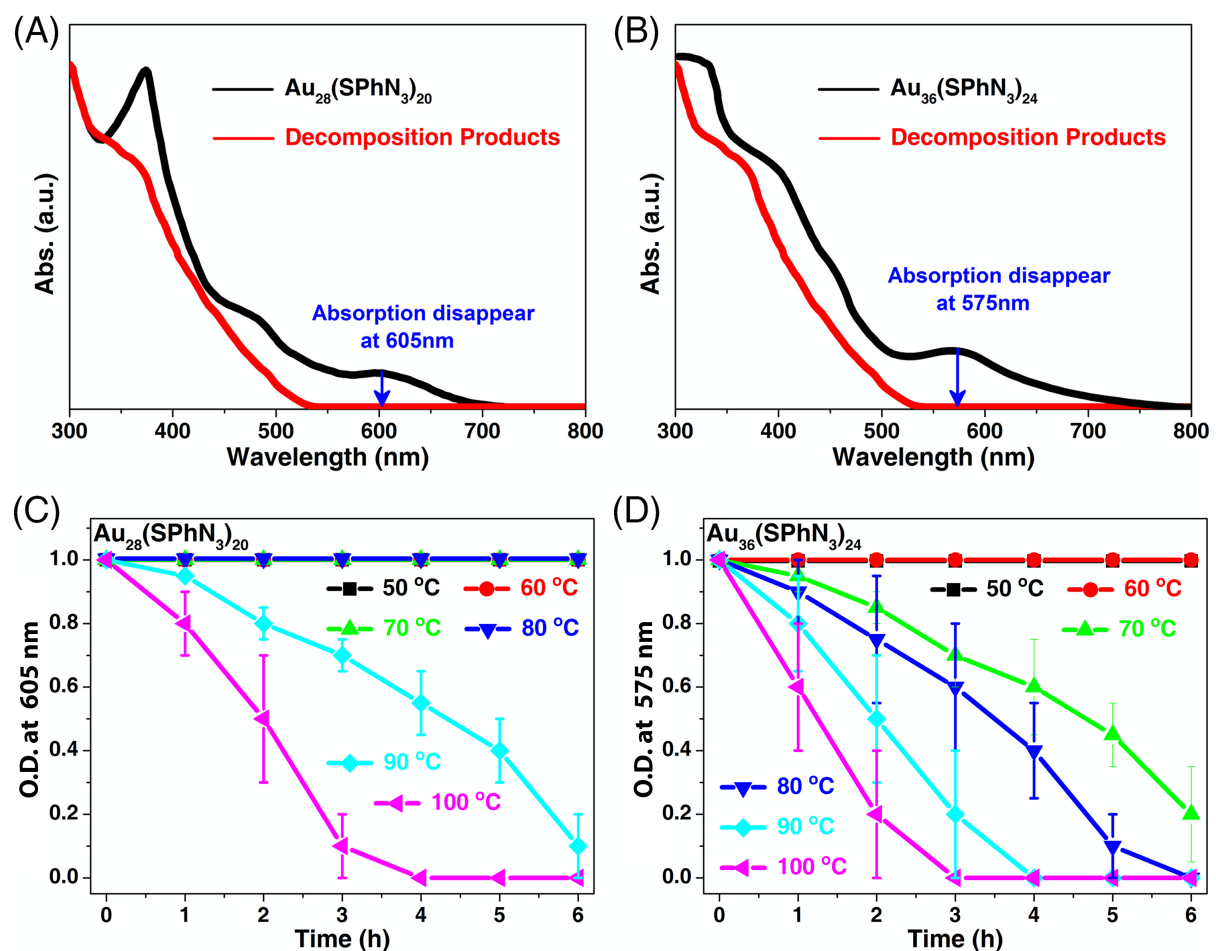


Figure S12. (A-B) UV-vis spectroscopy of clickable nanoclusters (black) and their decomposition products (red). (C-D) Stabilities of $\text{Au}_{28}(\text{SPhN}_3)_{20}$ and $\text{Au}_{36}(\text{SPhN}_3)_{24}$ as a function of heat treatment time and temperature, determined by the optical density at 605 nm and 575 nm, respectively.

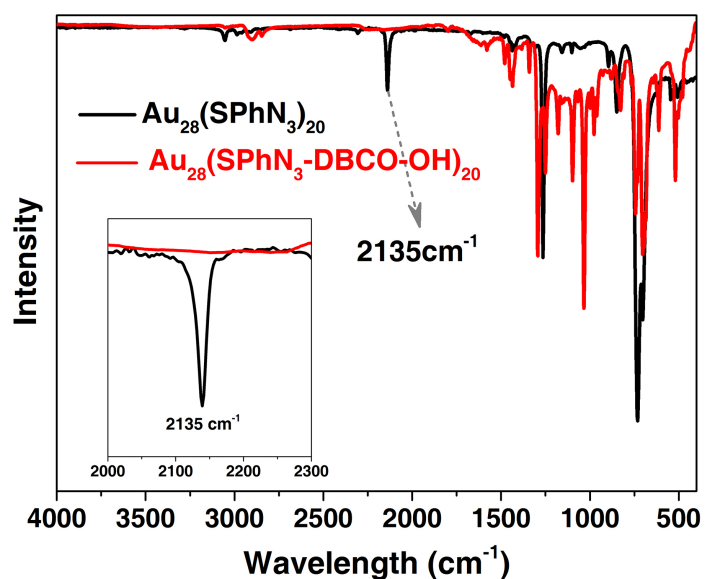


Figure S13. FTIR spectra of $\text{Au}_{28}(\text{SPhN}_3)_{20}$ (black) and $\text{Au}_{28}(\text{SPhN}_3\text{-DBCO-OH})_{20}$ (red). The absence of a 2135 cm⁻¹ vibration of $\text{Au}_{28}(\text{SPhN}_3\text{-DBCO-OH})_{20}$ indicates that all surface azide moieties are consumed by the click reaction.